NVH analysis and optimization of an electric powertrain

Analysis of an electric motor

Master's thesis in Applied Mechanics

VIGNESH SUBRAMANIAN

Department of Mechanics and Maritime Sciences

CHALMERS UNIVERSITY OF TECHNOLOGY
Gothenburg, Sweden 2022
www.chalmers.se

Master's thesis 2022

NVH analysis and optimization of an electric powertrain

Analysis of an electric motor

VIGNESH SUBRAMANIAN

CHALMERS
UNIVERSITY OF TECHNOLOGY

Department of Mechanics and Maritime Sciences
Division of Dynamics
Chalmers University of Technology
Gothenburg, Sweden 2022

NVH analysis and optimization of an electric powertrain
VIGNESH SUBRAMANIAN

Supervisor : Ramkumar Kandasamy, NVH Engineer,Volvo CE

Examiner: Thomas Abrahammson, Mechanics and Maritime Sciences, Division of Dynamics, Chalmers University of Technology

Master's Thesis 2022:48.
Department of Mechanics and Maritime Sciences
Division of Dynamics
Chalmers University of Technology
SE-412 96 Gothenburg
Telephone +46 31 772 1000

Cover: Electric Powertrain plate

Typeset in LaTeX
Gothenburg, Sweden 2022

NVH analysis and optimization of an electric powertrain
VIGNESH SUBRAMANIAN
Department of Mechanics and Maritime Sciences
Chalmers University of Technology

Abstract

Because of its compact shape and high power density, the permanent magnet synchronous motor (PMSM) appears to be better as a drive motor for electric construction machines (ECMs). However, as compared to conventional construction machines, the motor-driven machine has exhibited a different noise profile as a result of the shift in noise excitation source. The dramatic increase in high-frequency noises is particularly noticeable in this scenario. Furthermore, some of these high-frequency noises are distributed in the frequency range that is sensitive to human hearing, causing operators to feel highly uneasy.

Furthermore, gear whine noise emitted from the electric powertrain system could significantly affect driving comfort and has become an important NVH problem. The motor's electromagnetic forces and the reducer's gear-meshing forces could create structural vibration and whining noise with clear order characteristics. As a result, it's critical to look into the NVH characteristics of PMSM and reducer for ECMs. Computer-aided engineering (CAE) based vibration and sound simulation is a key approach for studying and optimizing electric powertrain NVH behavior, especially in the early stages of design. To put it another way, being able to forecast the noise and vibration harshness (NVH) behavior of an electric drive used in ECMs without having to run experimental solutions can save a company a lot of time and money.

Keywords: NVH, PMSM, Electric Motor, ECMs, Powertrain

PREFACE

The Master Thesis project work is carried out from February 2022 to June 2022 with Volvo CE at Volvo CE, Eskilstuna. The project is supervised by Ramkumar Kandasamy at Volvo CE and examined by Thomas Abrahamsson at the Chalmers University of Technology.

ACKNOWLEDGEMENTS

I would sincerely like to thank my supervisor Ramkumar Kandasamy, NVH engineer at Volvo CE, for his continuous support during the entire duration of the master thesis project. The technical knowledge and input he provided about powertrains and electric motors were crucial to the completion of the project on time. The timely access to all the necessary software were particularly useful to compare the results

I would also like to express my gratitude to Magnus Bjork, manager, Transmissions department, Volvo CE, for his unwavering support through out the master thesis

I would like to extend my gratitude to Thomas Abrahammson,Full professor, Division of Dynamics, for his valuable inputs during the entire course of the master thesis.

I would also like to thank my thesis partner at Volvo CE, Anujit Dafle, for his support through the thesis work.

Vignesh Subramanian, Gothenburg, June 2022

NOMENCLATURE

I_{peak}	-	Maximum phase current in the circuit
γ	-	Control angle
E	-	Electric field
ρ	-	Volume charge density
ε	-	Electric constant
B	-	Magnetic flux density
μ_0	-	Magnetic constant
J	-	Total current density
σ	-	Magnetic stress tensor
ρ_0	-	Density of air
c	-	speed of sound
V_n	-	structuralnormal velocity of the vibrating structure
A	-	surface area of the vibrating structure
P	-	Power loss of the control volume
f	-	Frequency
k,a,b	-	Steinmetz coefficients

Contents

List of Figures

List of Tables

1

Introduction

1.1 Background

Noise and vibrations of electrical machines are mainly due to electromagnetically excited sources (magnetostriction and Maxwell forces) and mechanical sources. Sources of electromagnetic vibrations have the cogging torque, torque ripple, and time-varying traction. Sources of mechanical vibration have rotor dynamic, rotor unbalance, bearings, flexible shaft etc. The radial force, which is a force between the rotor and stator in the excited state, also affects the NVH characteristics. In order to reach the specific NVH targets, methods based on computer-aided engineering (CAE) have to be developed for electric motors both for mastering the excitations from electromagnetic sources and for improving the NVH responses from the whole powertrain structure. The CAE simulation process for investigating NVH of electric powertrain is shown in Figure

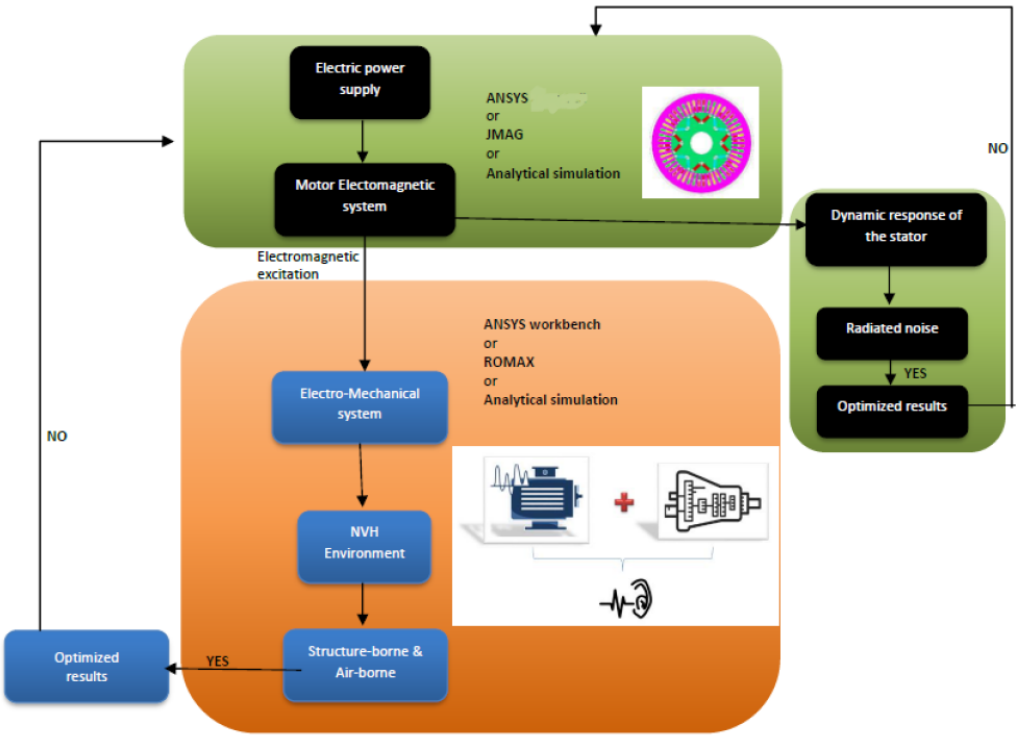

Figure 1.1: Flowchart

1.2 Purpose

NVH Analysis of an Electric powertrain is a complicated process. Noise and Vibration arise from both the Electric Motor and Gearbox. Further, In the Electric motor alone, noise is originated from electromagnetic and mechanical sources. This thesis aims to investigate and describe a full CAE process for the NVH analysis and optimization of powertrains.

This thesis also aims to optimize the total noise being emitted from the motor by changing the parameters of the motor.

1.3 Limitations

The main limitation of the thesis is that the combination of electric motor and the power train cannot be analysed using the same software tools. MotorCAD and/or Ansys Maxwell is needed for generating the elctromagnetic forces and the results need to be coupled with Ansys Workbench for harmonic response analysis and acoustic analysis. It needs to be ensured that the forces are acting at the correct nodes as the imported loads may not be assigned to the correct nodes.

Another limitation which was faced during this thesis work is that a 2D model of the motor was used for generating the electromagnetic forces whereas the acceleration response and acoustic analysis was done for the entire 3D model of the motor including stator and motor housing.

2

Theory

2.1 Electric Motor

The electric motor used in this thesis project is a Permanent Magnet Synchronous Motor (PMSM). A 2D model of a PMSM motor designed in MotorCAD is shown in the figure 2.1

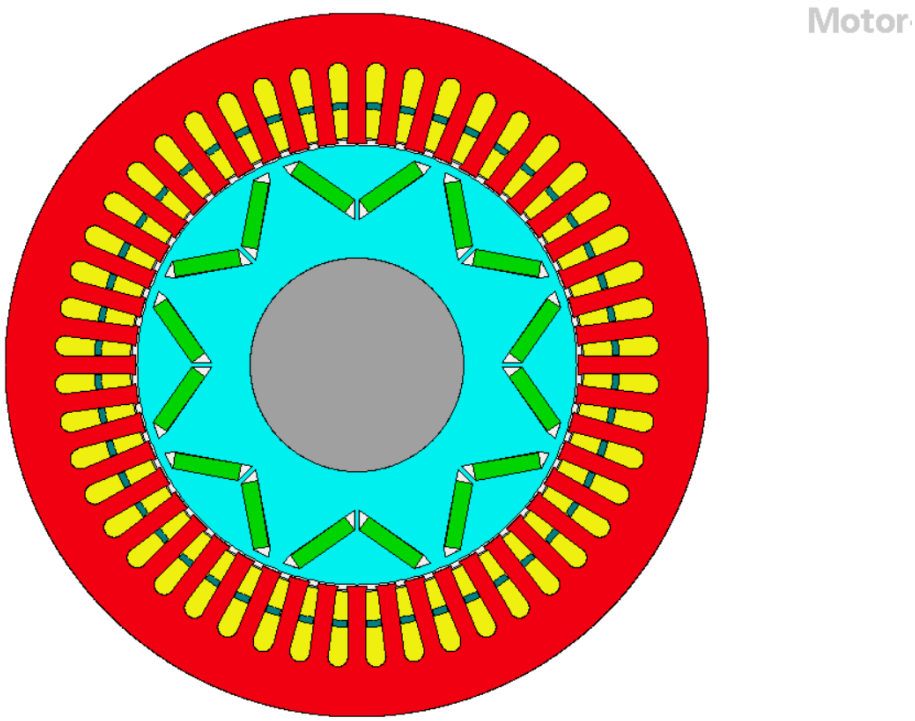

Figure 2.1: Electric Motor model in MotorCAD

The Permanent Magnet Synchronous Motor (PMSM) is an AC synchronous motor whose field excitation is provided by permanent magnets[1]. The PMSM is a combination of an induction motor and brushless DC motor. Permanent magnets are embedded on the rotor and windings are connected in the stator slots similar to a brushless DC motor. It also produces a sinusoidal flux density in the airgap between stator and rotor similar to an induction motor. The PMSM used in this thesis is a 3 phase, 8 pole motor with 48 stator slots. The different parts of the PMSM are explained in detail below.

2.1.1 Stator

The stator, as the name suggests, is the static part of the electric motor. It is one of the two primary components of the electric motor, the other one being the rotor. In AC motors, the stator is made up of slots into which insulated coils are placed. These coils are then connected to the power source. The coils then behave as an electromagnet. The north and south poles of the induced magnetic field of the coils are synced with the respective opposite poles present in the permanent magnets of the rotor, causing the rotor to rotate.

Stator Parameters	Value
Stator Lam Dia	mm
Stator Bore	mm
Number of Slots	slots
Tooth Width	mm
Slot Depth	mm
Slot opening	mm

Table 2.1: Stator Parameters

2.1.2 Rotor

The rotor is the rotating part of the electric motor. In PMSM, the rotors are embedded with permanent magnets. The rotation of the rotor is due to the interaction between the magnetic field produced by the windings and the magnetic field of the permanent magnets. This produces a torque around the rotors axis.

Rotor Parameters	Value
Number of Poles	poles
Magnet Thickness	mm
Airgap	mm
Shaft dia	mm
Shaft hole dia	mm

Table 2.2: Rotor Parameters

The stator and rotor are shown in the Figure 2.1

2.1.3 Windings

In electric motor, windings are the wires present inside the stator slots in the shape of coils. The connection of the windings between the different slots and the position of the windings inside a slot are shown below :

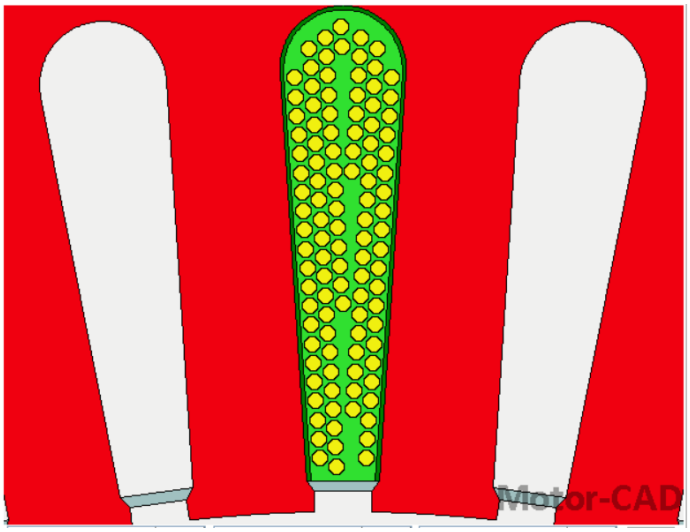

Figure 2.2: Windings inside stator slot

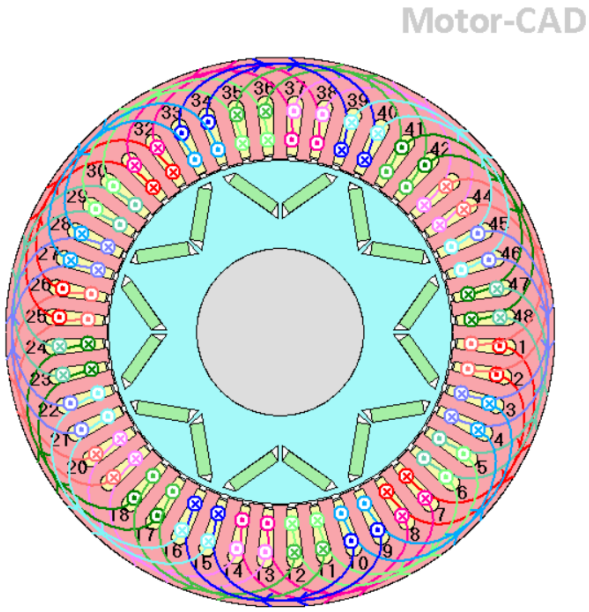

Figure 2.3: Connection between stator slots

The three phase current passes through the windings. The figure below shows the current fluctuations in the three phases:

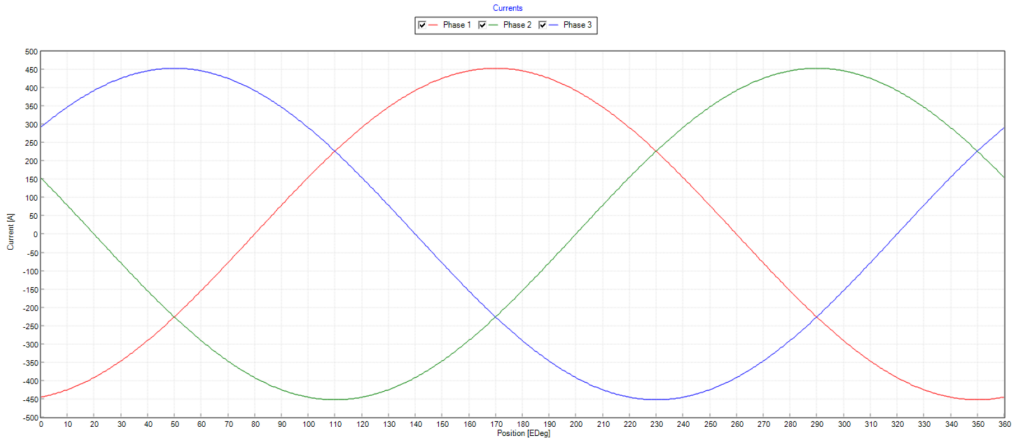

Figure 2.4: The current in three phases

The current in the three phases are defined by the equations:

$$Phase\ A = I_{peak} * sin(\frac{2pi}{60} * rpm * time + \gamma) \tag{2.1}$$

$$Phase\ B = I_{peak} * sin(\frac{2pi}{60} * rpm * time - 120 + \gamma) \tag{2.2}$$

$$Phase\ C = I_{peak} * sin(\frac{2pi}{60} * rpm * time - 240 + \gamma) \tag{2.3}$$

where I_{peak} is the maximum phase current in the circuit, rpm is the machine rpm and γ is the control angle.

2.1.4 Motor Noise and Vibration Mechanisms

The total noise and vibration from an electric motor can be split into two components, namely noise and vibration from mechanical causes and noise and vibration from electromagnetic causes [14].

The sources of Mechanical causes include :

- Bearings
- Shaft imbalance
- Shaft eccentricity
- Sliding contacts

The sources of Electromagnetic causes include :

- Maxwell forces - Radial and Tangential forces acting on the stator teeth in the airgap between stator and rotor
- Torque ripple

In this thesis, we only focus on the noise and vibration from electromagnetic causes [13].

2.1.5 Maxwell Equations and Stress tensor

Maxwell's equations consist of four partial differential equations that forms the basis of classical electromagnetism [11]. They are classified as:

Gauss Law
Gauss's law is a relation between the electric charge and the corresponding electric field. It is defined by the equation:

$$\nabla \cdot \mathbf{E} = \frac{\rho}{\varepsilon_0} \tag{2.4}$$

where $\mathbf{E}$ is the electric field, ε_0 is the electric constant ρ is the volume charge density

Gauss's law for magnetism
Gauss's law for magnetism states that the divergence of a magnetic field is always equal to zero. It is defined by the equation:

$$\nabla \cdot \mathbf{B} = 0 \tag{2.5}$$

where $\mathbf{B}$ is the magnetic flux density.

Faraday's law of induction
Faraday's law of induction describes the phenomenon known as Electromagnetic Induction. It states that a varying magnetic flux passing through the surface enclosed by a current carrying loop will induce a electromotive force in the conductive loop [15]. It is defined by the Maxwell–Faraday equation which gives the relation between the magnetic field and the electric field [15].

$$\nabla \times \mathbf{E} = -\frac{\partial \mathbf{B}}{\partial t} \tag{2.6}$$

where $\mathbf{E}$ is the electric field and $\mathbf{B}$ is the magnetic field.

Ampère's circuital law
Ampère's circuital law gives the relation between the current flowing through a closed loop and the magnetic field surrounding the closed loop. The relation is given by the equation [16]:

$$\nabla \times \mathbf{B} = \mu_0 \left(\mathbf{J} + \varepsilon_0 \frac{\partial \mathbf{E}}{\partial t} \right) \tag{2.7}$$

where $\mathbf{B}$ is the magnetic field, $\mathbf{E}$ is the electric field and $\mathbf{J}$ is the total current density.

Using Equations (2.4), (2.5), (2.6) and (2.7), the Maxwell Stress Tensor can be formulated which contains every aspect of electromagnetism. The Maxwell Stress Tensor is given in SI units by [17]:

$$\sigma_{ij} \equiv \varepsilon_0 \left(E_i E_j - \frac{1}{2}\delta_{ij} E^2 \right) + \frac{1}{\mu_0} \left(B_i B_j - \frac{1}{2}\delta_{ij} B^2 \right) \tag{2.8}$$

where ε is the electric constant, μ_0 is the magnetic constant and δ_{ij} is the Kronecker's delta. The Maxwell stress tensor is calculated considering both the electric and magnetic fields. For only electric or magnetic fields, the Maxwell stress tensor can be simplified further.

2.1.5.1 Radial and Tangential Forces

In a motor, since the magnetic field is the significant contributor towards the Maxwell stress tensor, it can be simplified to [17]:

$$\sigma_{ij} = \frac{1}{\mu_0} B_i B_j - \frac{1}{2\mu_0} B^2 \delta_{ij} \tag{2.9}$$

For a motor, the i, j terms are replaced by r, t where r is the radial and t is the tangential component. The Equation (2.9) can hence be written as:

$$\sigma_{rt} = \frac{1}{\mu_0} B_r B_t - \frac{1}{2\mu_0} B^2 \delta_{rt} \tag{2.10}$$

2.1.5.2 Torque Ripple

Torque ripple occurs when the torque is not a constant value but is rather interrupted by a periodic disturbance which causes a periodic increase or decrease in the output shaft as the motor rotates.
The main reason for the Torque ripple in a PMSM is the cogging torque. Since the stator is also made of metal, there would be an interaction between the Permanent magnets of the rotor and the stator. Cogging torque is the torque needed to overcome this interaction [18].

2.1.6 Equivalent radiated Power

Equivalent radiated Power (ERP) is a criteria to evaluate structure borne noises [12]. ERP enables the user to estimate how the vibrations of a structure are converted to structure borne noise. ERP is given by the formula :

$$\text{ERP} = \frac{1}{2} \rho_0 c \int_A |v_n|^2 \, dA \tag{2.11}$$

where ρ_0 is the density of air, c is the speed of sound in air, v_n is the structural normal velocity of the vibrating structure, and A is the surface area of the vibrating structure.

It should be noted that the ERP estimation is accurate only for low frequencies, especially the first resonance frequency. For higher frequencies, the movement of the structure has different phase relations and so acoustic short-circuits appear [12]. This means that the sound waves undergoes destructive interference and the sound waves cancel out each other.

3

ELECTROMAGNETIC SIMULATION

In this section, the software used and the different load cases used will be explained. The entire process of the simulation of the electric motor, modal analysis, harmonic response analysis and acoustic analysis will also be explained in detail.

3.1 Software

3.1.1 MotorCAD

Motor-CAD is an Electromagnetic and Thermal analysis package for electric motors and generators, developed and sold by Motor Design Ltd [2]. The advantages of using MotorCAD are

- Predefined templates of different types of motors available. A model can be created without hassle by entering the required values
- The different model environments, namely E-magnetic, Thermal, Lab and Mechanical allow the user to setup and study the post process data according to different operating conditions

The functions and purpose of each of the model environments is explained below: [3]

E-Magnetic
- Calculates the Maxwell forces, torque, Flux linkages etc
- Can be coupled with Thermal solver

Thermal
- Calculates the temperature of components under operating conditions
- Provides understanding of heat transfer paths

Lab
- Calculates efficiency maps, maximum torque/speed curve
- Perform duty cycle analysis

Mechanical
- Calculates rotor stress

- Can also be used for structural and acoustic analysis

However, it is difficult to study the results of the electric motor with an user designed housing. This is why Ansys Electronics desktop and Workbench is also used.

3.1.2 Ansys EDT and Workbench

Once a model is generated in MotorCAD, it is easy to export it to Ansys EDT. Ansys EDT is used since harmonic force calculation can be enabled. Electromagnetic simulations are run in Ansys EDT to find the radial, tangential forces and the torque ripple. Once the electromagnetic simulation is done in Ansys EDT, it can be exported to workbench where the results can be coupled with Modal, harmonic response and acoustic analysis. The workflow of the entire process is shown below :

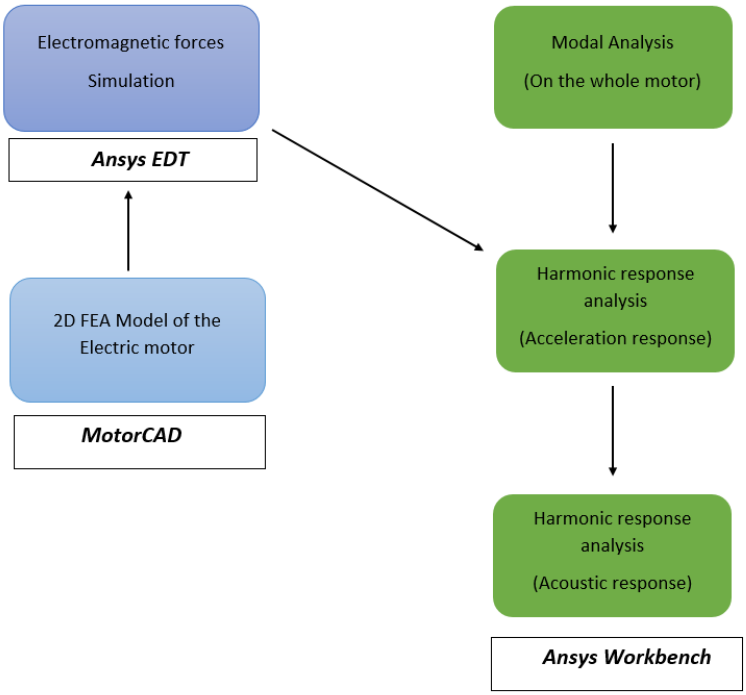

Figure 3.1: Flowchart showing the workflow

3.2 Generating the Model - MotorCAD

As explained in section 3.1.1, MotorCAD generates a 2D model of an electric motor using predefined templates using input parameters.

3.2.1 E-Magnetic

3.2.1.1 Stator and Rotor

In the E-Magnetic model, Finite element analysis is done on the electric motor and the back emf, cogging torque and magnetic flux density is plotted. The first step is

to create the geometry of the stator and rotor. It is done by using the geometric parameters in Tables 2.1 and 2.2. The materials for stator and rotor are chosen from the MotorCAD library. The material properties are as follows:

Property	Stator	Rotor
Material from database	Mxxx	Mxxx
Electrical resistivity (Ohm.m)	5xxx	5xxx
Density (kg/m^3)	xxxx	xxxx
Weight (Kg)	xx.xx	xx.xx

Table 3.1: Material properties of stator and rotor

3.2.1.2 Permanent Magnets and Windings

Next, we define the material properties of the permanent magnets.

Property	Permanent Magnet
Material from database	xxxx
Electrical resistivity (Ohm.m)	xxxx
Density (Kg)	xxxx
Weight (Kg)	xxxx

Table 3.2: Material properties of Permanent Magnets

Next is the winding definition. In this thesis, we use a lap winding with an upper-lower path type and stranded coil. The details are summarized in the table below.

Winding type	Lap
Path type	Upper-Lower
Coil	Stranded

Table 3.3: Winding definition

3.2.1.3 Mesh Control

For creating the mesh in MotorCAD, the mesh length for the stator, rotor and the airgap mesh must be specified. One complete rotation of the rotor is considered and solver used is the transient solver.

Part	Mesh setting
Stator mesh length	1 mm
Rotor mesh length	1 mm
Airgap layers	4
Airgap surface points	720
Airgap Internal points	720

Table 3.4: Mesh settings in MotorCAD

Since the radial, tangential forces and the toque ripple are acting in the airgaps, we have a finer mesh at those places than the stator and rotor.

3.2.1.4 Losses

Once the geometry of the motor, wingings and mesh are created, the losses occurring during the operation of the motor must be taken into account. There are three types of losses which can be specified in MotorCAD. They are listed below :

Iron Losses
The iron losses or core losses are calculated in MotroCAD using the Steinmetz method or Steinmetz's equation. Steinmetz's equation is an empirical equation used to calculate the total core losses in a magnetic material when an external varying sinusoidal magnetic field acts upon them. The losses are calculated according to the equation :

$$P = k.f^a.B^b \tag{3.1}$$

where P is the power loss per unit volume, f is the frequency in kilohertz, B is the maximum magnetic flux density and k,a,b are called Steinmetz coefficients. They are material properties which is found from the materials B-H curve.

Bearing Losses
The Bearing losses are given as a direct user input as these values have been obtained experimentally. The bearing losses are shown in the graph below :

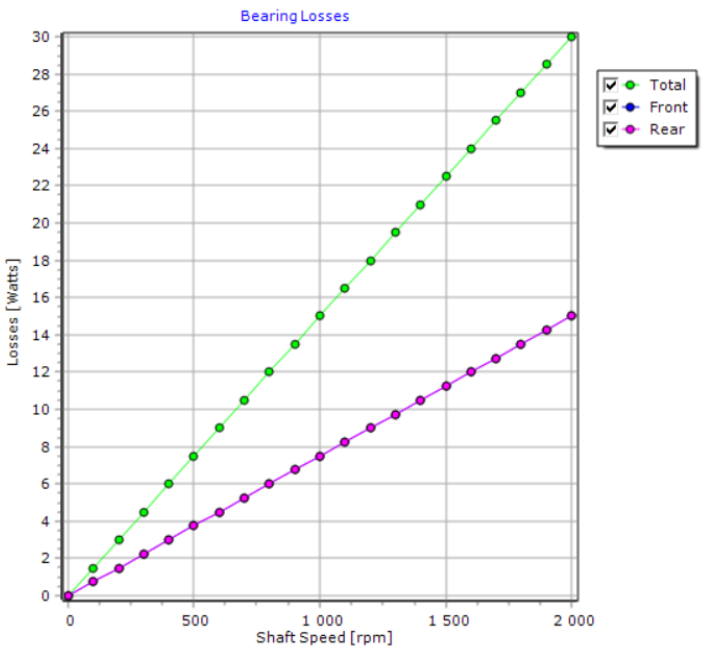

Figure 3.2: Bearing losses

AC Winding Losses
To calculate the AC Winding losses, Hybrid FEA loss model is chosen.

3.2.1.5 Input Parameters

The last step before running the E-Magnetic simulation is to give the input parameters of the motor. They are mentioned in the table given below. All the values were provided by Volvo CE.

Input Parameter	Value
Shaft Speed	rpm
Peak current	A
RMS current	A
Winding temperature	deg celcius
Magnet temperature	deg celcius
Shaft temperature	deg celcius

Table 3.5: Input parameters

Once the entire model of the motor is defined, the electromagnetic model can be solved. The magnetic flux density at 2000rpm and 425Nm torque is shown below.

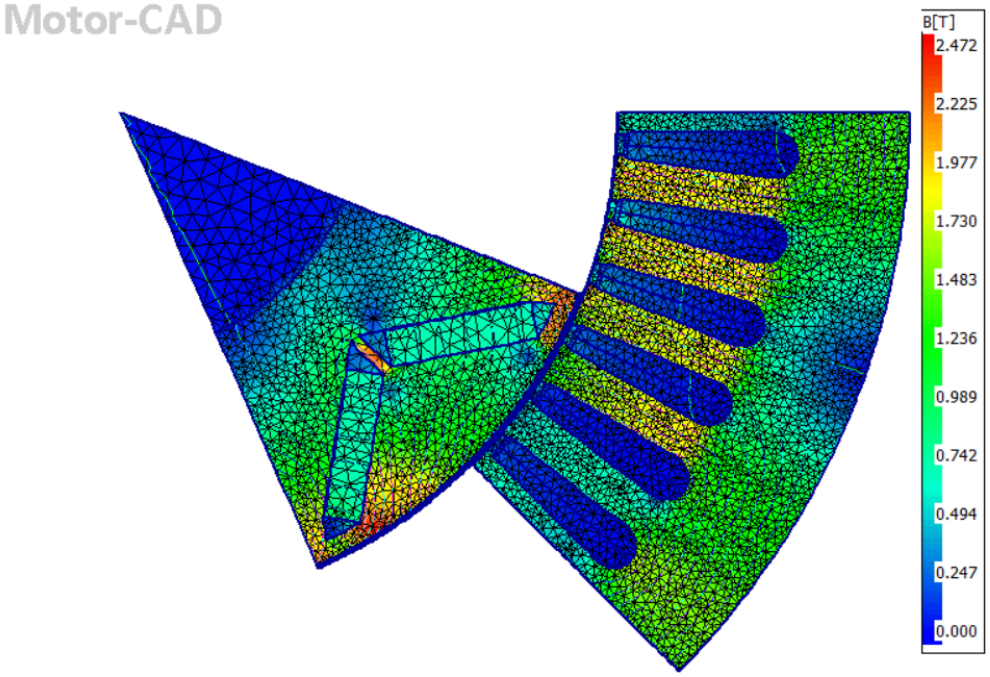

Figure 3.3: Magnetic flux density at 2000 rpm and 425 Nm torque

Stator tooth	1	2	3	4	5	6
Radial Force (N)	-0.06F_r	-F_r	-0.76F_r	-0.83F_r	-0.305F_r	-0.062F_r
Tangential Force(N)	-0.019F_t	-0.214F_t	-F_t	-0.56F_t	-0.139F_t	-0.005F_t

Table 3.6: Radial and Tangential force acting on the stator teeth at 2000 rpm and 425 Nm

The Table 3.6 shows the normalized radial and tangential force acting on the stator tooth at 2000 rpm and 425 Nm, where F_r is the normalizing factor for the radial force and F_t is the normalizing factor for the tangential force. It can be observed that the radial force is significantly higher than tangential force. This is due to the magnetic flux lines being more concentrated in the radial direction than tangential direction.

3.2.2 Lab

As mentioned in section 3.1.1, the lab module calculates the maximum torque/speed curve of the motor. The load points requested from Romax are shown in the table 3.7 below. V_{ideal} is the ideal operating speed of the motor.

Requested Torque (Nm)	Speed (rpm)
425	$0.023V_{ideal}$
425	$0.47V_{ideal}$
425	V_{ideal}
310	$1.42V_{ideal}$
241	$1.9V_{ideal}$
150	V_{ideal}
186	$2.38V_{ideal}$

Table 3.7: Requested torque points from Romax

The model is built for the above load points and the torque envelope plot is shown below:

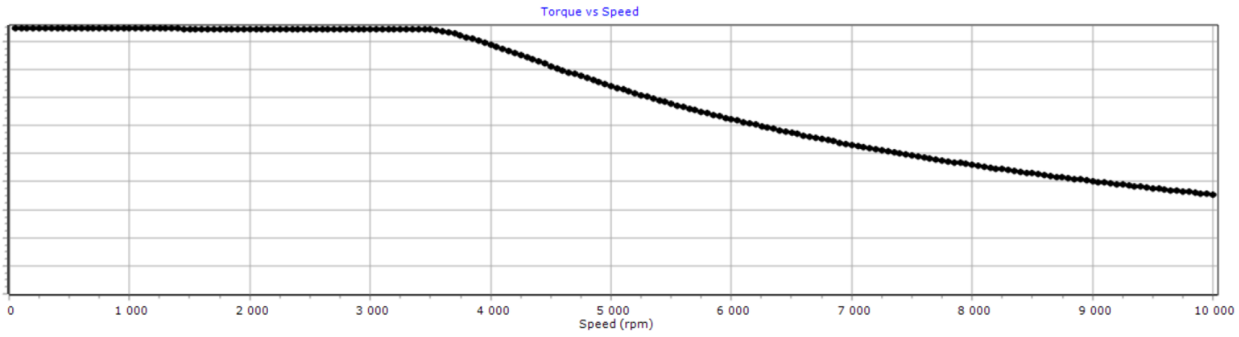

Figure 3.4: Torque Envelope for the given load points

3.2.3 Mechanical

Once the model is built, the simulation can be run in the Mechanical environment to find the calculated torque, peak line current and phase advance. The results of the same are shown below :

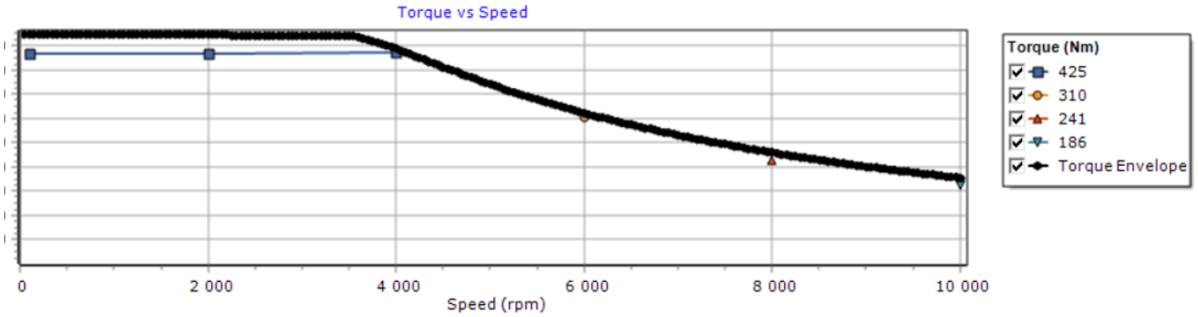

Figure 3.5: Calculated Torque

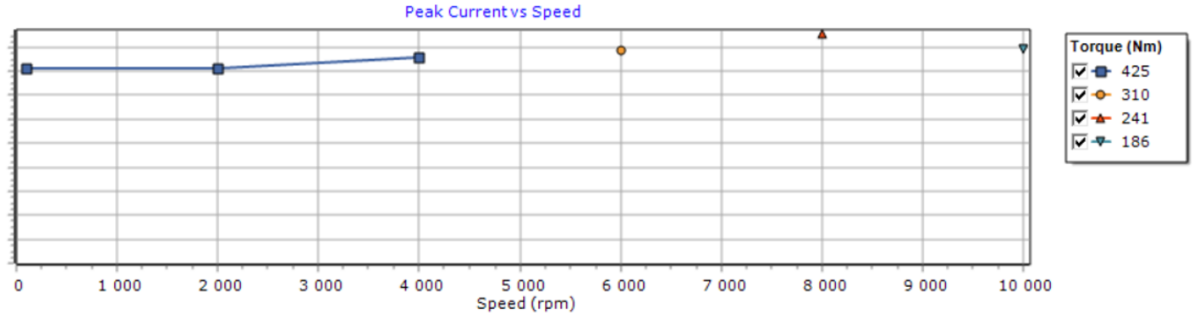

Figure 3.6: Peak line current

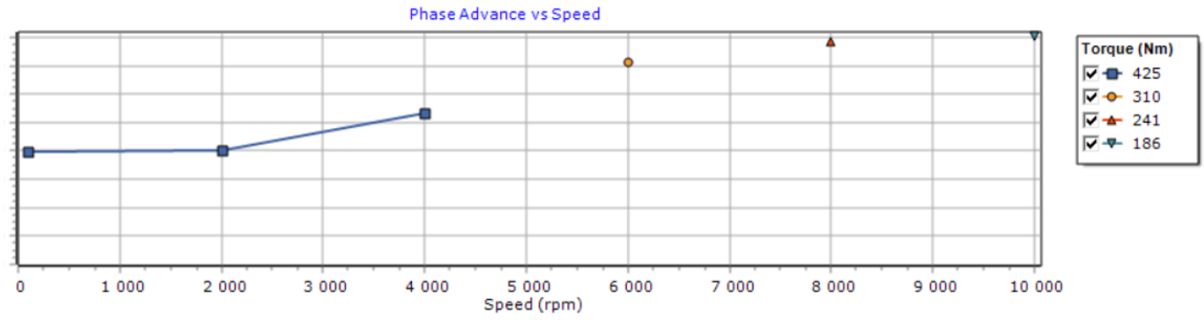

Figure 3.7: Phase Advance

It can be seen from Figures 3.6 and 3.7 that Peak line current and Phase Advance increases as the rpm increases. This is due to the induced back emf in the windings. The result from these simulations, namely the electromagnetic forces and torque, are then given as input to Romax for the NVH analysis on the powertrain. The model can be imported to Ansys EDT for coupling with Ansys Workbench for acceleration response analysis and acoustic analysis.

3.3 Ansys EDT

Once the model has been generated in MotorCAD, it can be imported to Ansys EDT along with stator, rotor, magnets and winding definitions. The imported model in Ansys EDT is shown below:

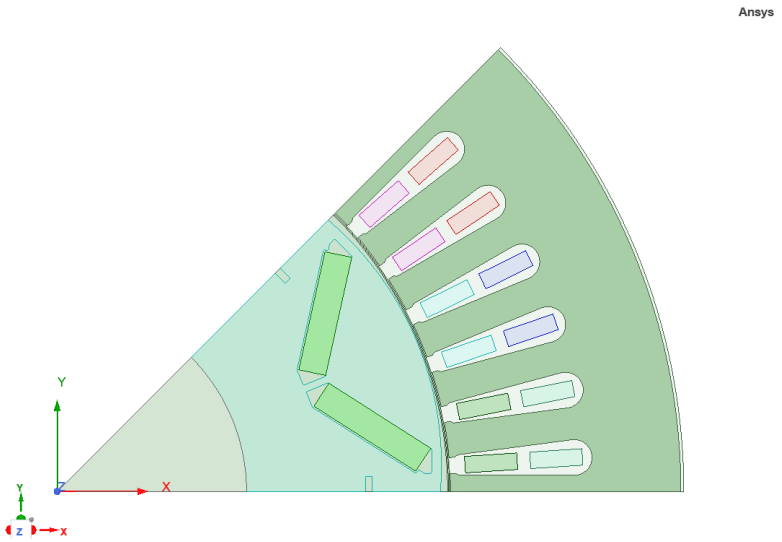

Figure 3.8: Imported motor model in Ansys EDT

As seen in Figure 3.8, the model in Ansys EDT has been reduced to 1/8 th of its actual size. This is because Ansys EDT considers symmetry and the results of the 1/8 th model can be extrapulated to get the results of the entire model.

4

NVH ANALYSIS AND RESULTS

The electromagnetic results from Ansys EDT are coupled with the motor model along with the housing in Ansys Workbench. In Ansys Workbench, Modal analysis is first performed to obatin the resonance frequencies. Acceleration response analysis and acoustic analysis are then performed to find the total noise emitted from the motor.

4.1 Mesh and Contact settings

The model of the motor along with the housing are shown in the figure below:

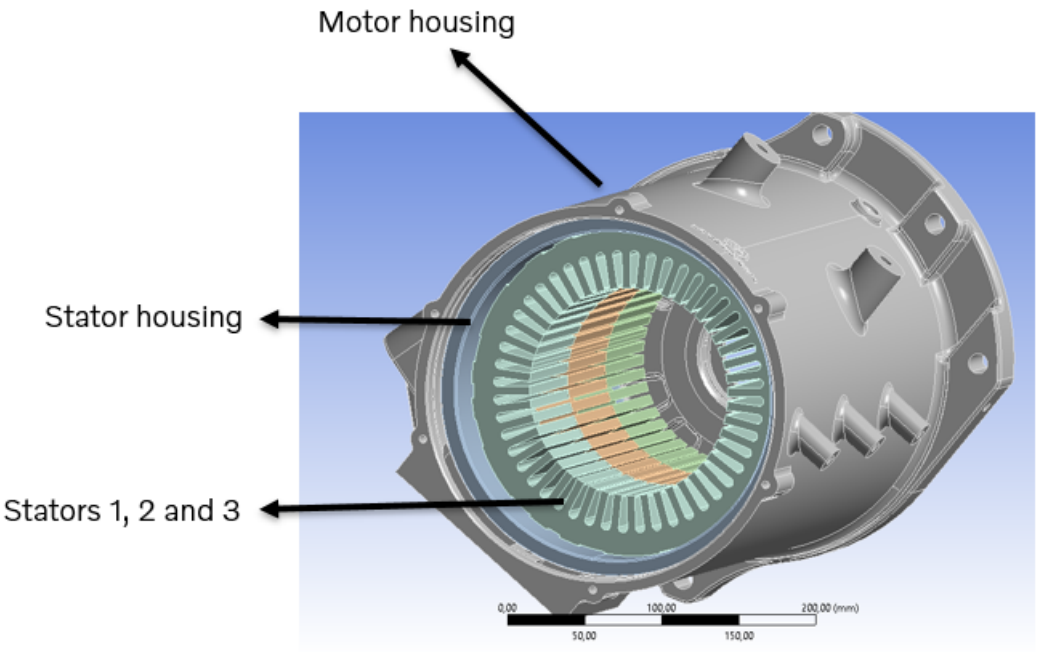

Figure 4.1: Motor model with housing in Ansys Workbench

Contacts are defined between the different components of the motor. They are

summarised in the table shown below:

Body 1	Body 2	Connection
Stator housing	Motor Housing	Bonded
Stator housing	Stator 1	Bonded
Stator housing	Stator 2	Bonded
Stator housing	Stator 3	Bonded
Stator 1	Stator 2	Bonded
Stator 2	Stator 3	Bonded

Table 4.1: Contacts between different components of the motor

Three different mesh sizes are used in the model.They are shown in the table below :

Component	Mesh size
Motor housing	4 mm
Stator housing	4 mm
Stators 1, 2 and 3	3 mm

Table 4.2: Mesh settings

A coarser mesh size is chosen for the motor and stator housing and a finer mesh is chosen for the stators since those are the main components which have to be investigated. The physical preference of the mesh property is chosen as mechanical to achieve the vibration mode shape. Adaptive sizing of the mesh is used. The mesh for the entire model is shown in the figure below :

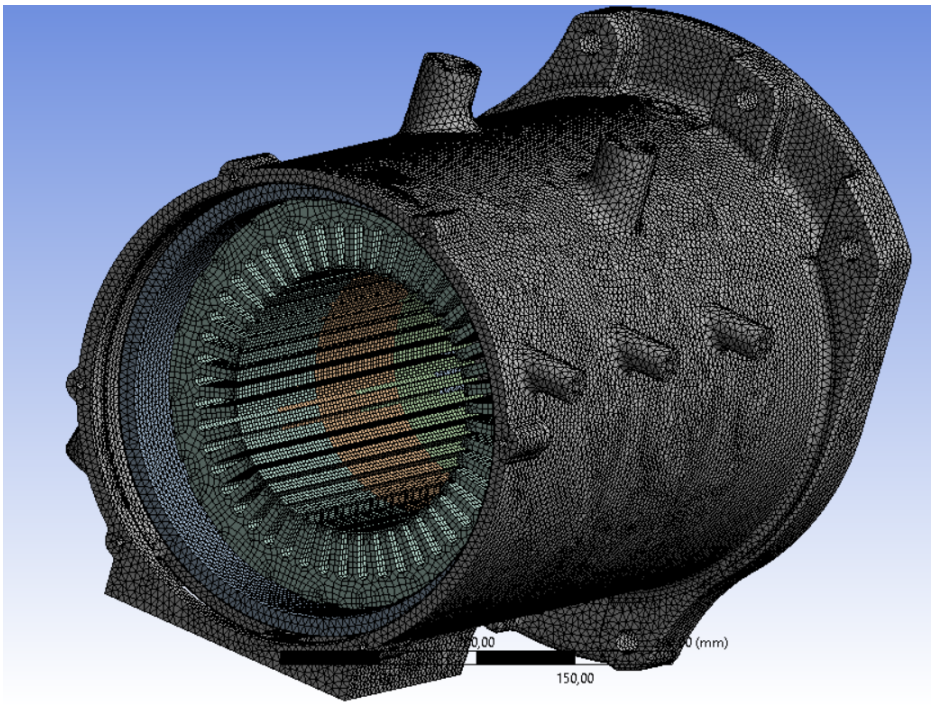

Figure 4.2: Mesh of the entire model

The motor is held at the locations shown Figure 4.3 to fix its position in the test rig. This is replicated in the model by assigning fixed supports at the given nodes.

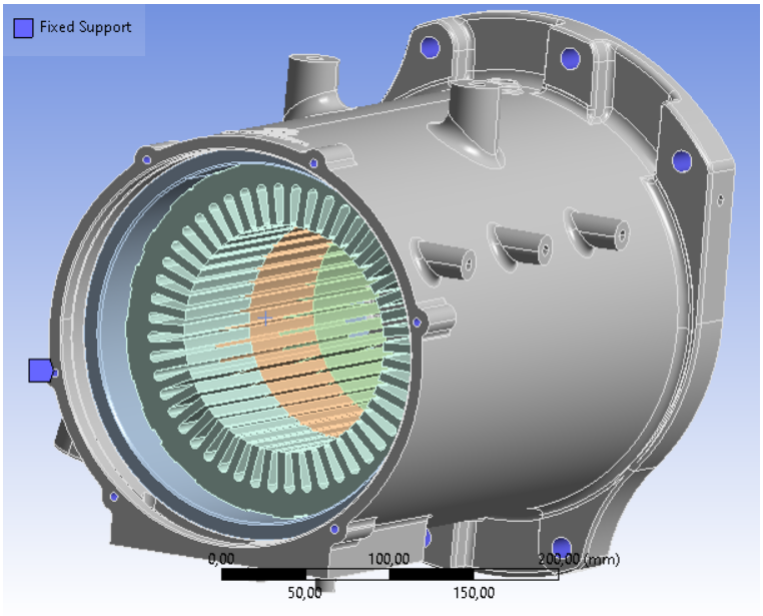

Figure 4.3: Fixed support at the motor housing

4.2 Loads

The electromagnetic forces are directly imported from Ansys Maxwell. These forces act on the surface of the stator teeth.

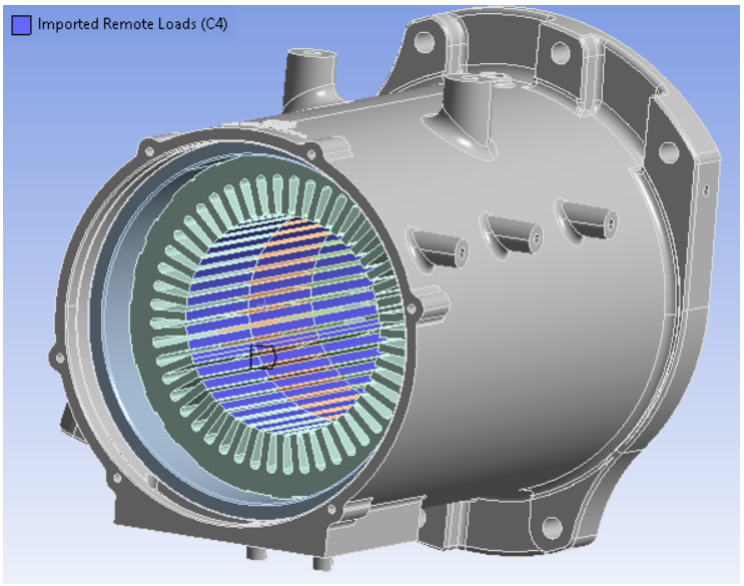

Figure 4.4: Imported loads on Stator teeth

4.3 Modal Analysis

Modal Analysis is performed on the motor to find the resonance frequencies. The first ten resonance frequencies upto 3200 Hz are considered are these are the frequencies which gave the maximum radial and tangential force values on the stator teeth. The results of the modal analysis are shown in the table 4.3 below, where $F_{1^{st}}$ is the first resonance frequency.

Mode	Frequency(Hz)
1	$F_{1^{st}}$
2	$1.05F_{1^{st}}$
3	$1.11F_{1^{st}}$
4	$1.2F_{1^{st}}$
5	$1.38F_{1^{st}}$
6	$1.8F_{1^{st}}$
7	$1.82F_{1^{st}}$
8	$1.85F_{1^{st}}$
9	$1.88F_{1^{st}}$
10	$1.92F_{1^{st}}$

Table 4.3: First 10 resonance frequencies of the motor

The plots sowing the maximum displacement at these frequencies are shown in Appendix 1.

4.4 Acceleration response and Acoustic analysis

The acceleration response analysis is done for two different rpms with the airgap between stator and rotor fixed as 0.625 mm. The entire outer surface of the stator is considered for the analysis. This is because a physical test has not yet been performed and the exact nodes where the sensors will be attached for measurements are not known. Hence, the entire surface was considered. Also, the acoustic analysis was done on the surface of the motor since during a physical test sensors would be attached to the surface of the motor.

RPM	Airgap (mm)
2800	0.625
4200	0.625

Table 4.4: Load cases

4.4.1 2800 RPM and 0.625 mm Airgap

The results for the acceleration response analysis and acoustic analysis for 2800 rpm and 0.625 mm airgap is shown below:

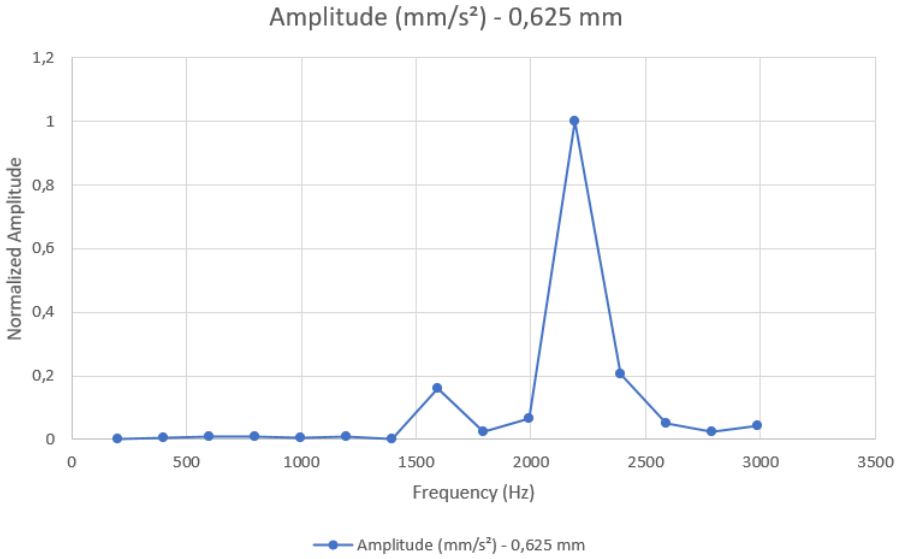

Figure 4.5: Acceleration response analysis for 2800 rpm and 0.625 mm airgap

It can be observed that the peak acceleration occurs after 2000 Hz. There is also a smaller peak occurring near 1600 Hz. The smaller peak is obtained close to the first resonance frequency and the highest peak is close to the resonance frequency which gives the maximum deformation, refer Table 4.3.

Equivalent Radiated Power

As mentioned in section 2.1.6, Equivalent Radiated Power gives an estimate about the frequencies at which maximum sound may be emitted.

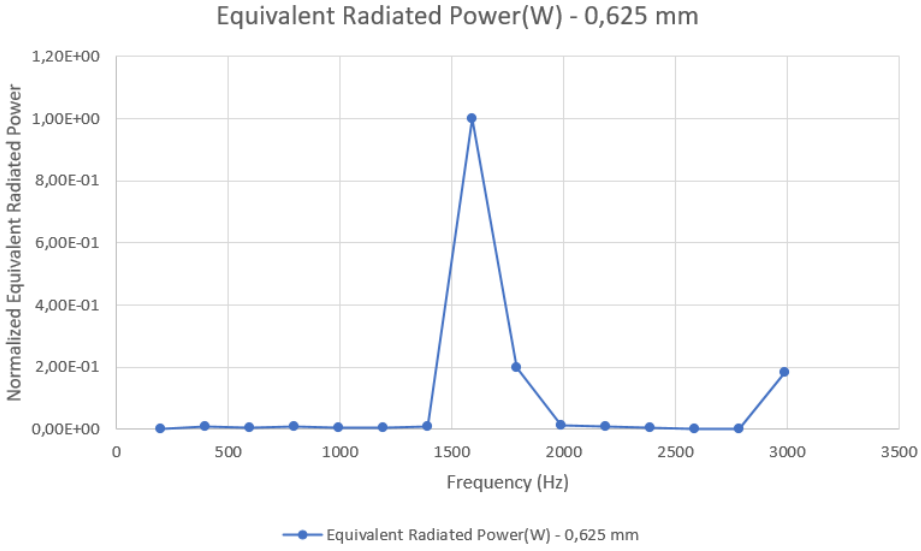

Figure 4.6: Equivalent Radiated Power for 2800 rpm and 0.625 mm airgap

From Figure 4.6, we can see that the maximum noise can be emitted closer to the first resonance frequency. Even though the maximum acceleration during vibration occurs at a frequency higher than 2000 Hz, the maximum sound is not emitted at

that frequency. This is due to acoustic short circuit occurring at higher frequencies where the destructive interference of sound waves occur. This means that crest of one wave and the trough of another occur at the same instance.

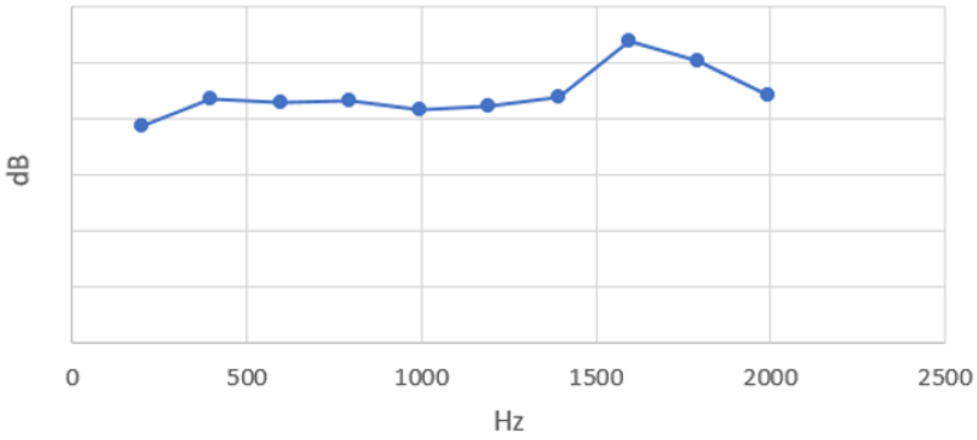

Figure 4.7: Sound emitted from the motor at 2800 rpm and 0.625 mm airgap

The Figure 4.7 supports the idea that the maximum sound will be emitted closer to the first resonance frequency. The waterfall diagram showing the variation of sound emitted with respect to different frequencies and rpm are shown in the image below:

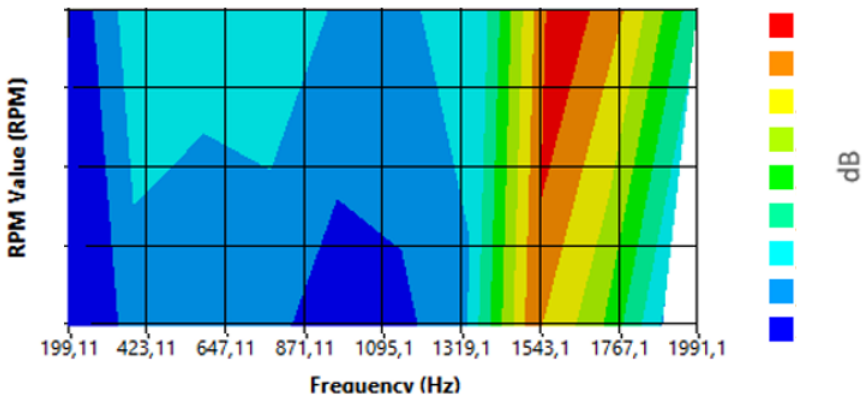

Figure 4.8: Waterfall diagram for 2800 rpm and 0.625 mm airgap

The Figure 4.8 shows that the highest sounds emitted from the motors are close to the range of the first resonance frequency.

4.4.2 4200 RPM and 0.625 mm Airgap

In this section, the RPM value is increased to 4200 and the results are analysed and compared with the results obtained for 2800 RPM. The Figure below shows the comparison between the acceleration response for the two RPMs:

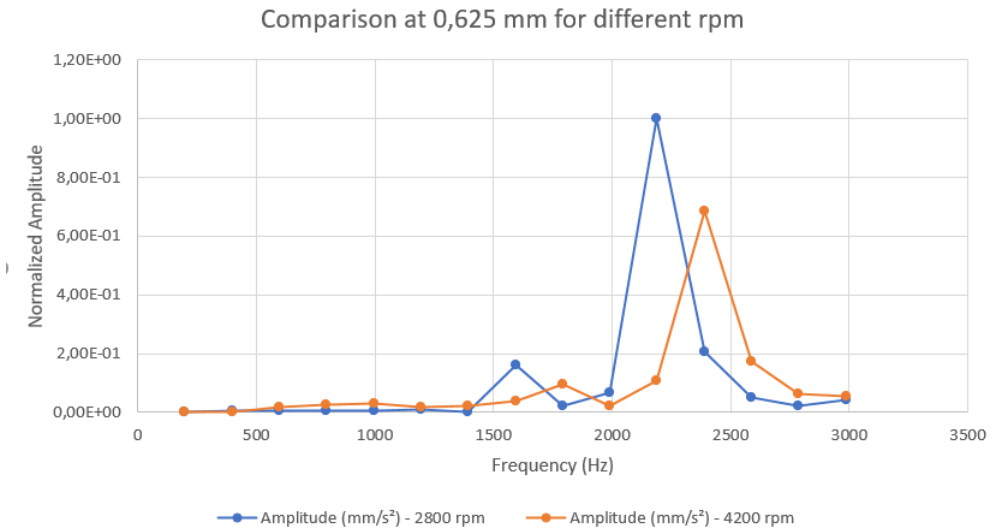

Figure 4.9: Comparison of Acceleration response 2800 rpm and 4200 RPM for 0.625 mm airgap

It can be seen from Figure 4.9 that though both the plots follow a similar trend, the peaks for 4200 rpm are lower and is obtained at a later frequency. This can be explained due to the fact that back emf are induced in the coils at higher speeds which decreases the electromagnetic forces acting on the stator teeth.

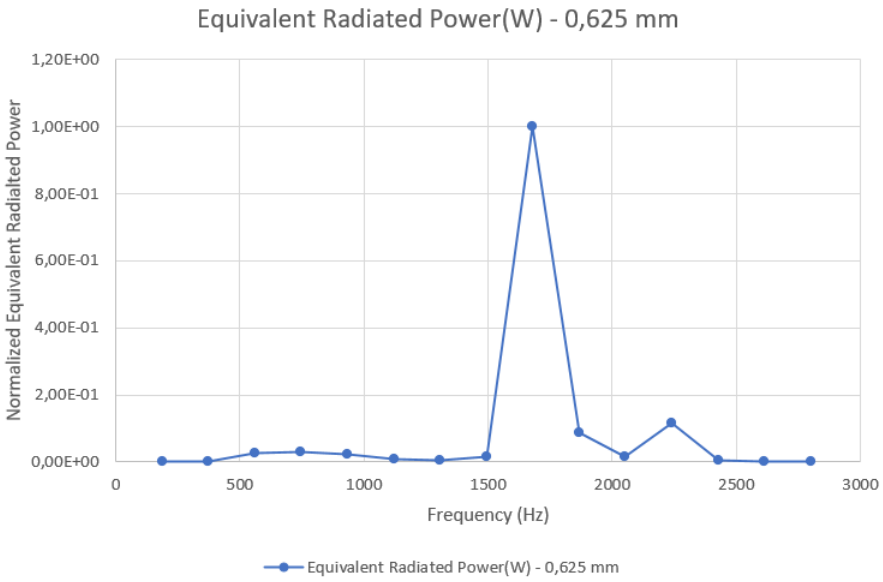

Figure 4.10: Equivalent Radiated Power at 4200 RPM and 0.625 mm airgap

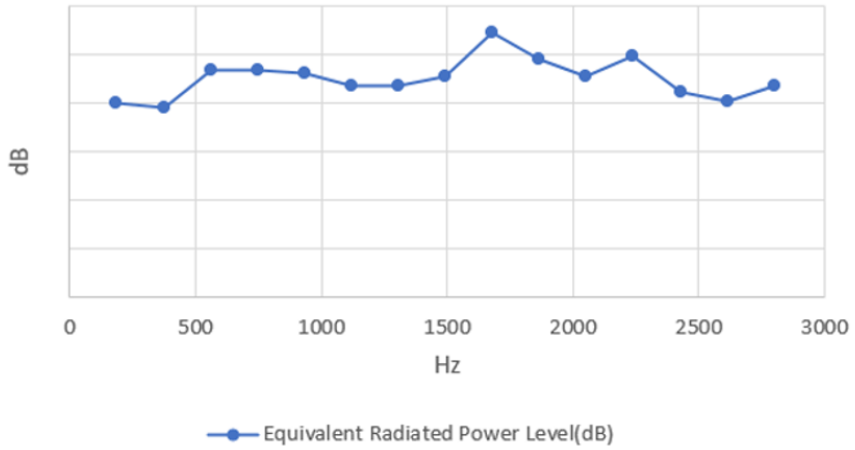

Figure 4.11: Sound emitted from the motor at 4200 RPM and 0.625 mm airgap

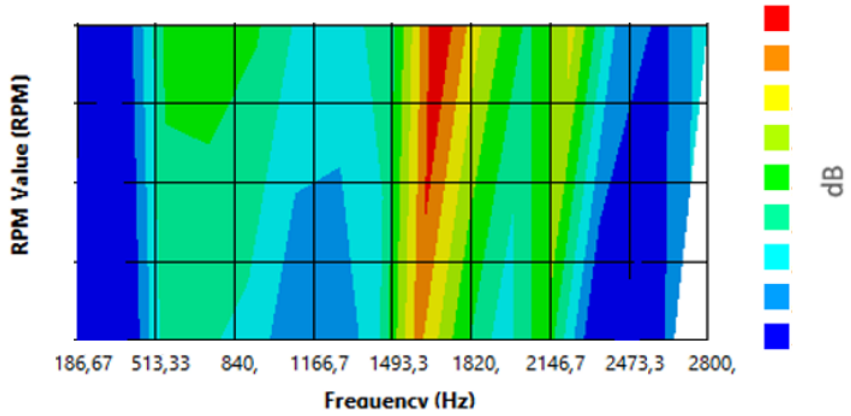

Figure 4.12: Waterfall diagram for 4200 RPM for 0.625 mm airgap

4.5 Optimization

To perform an optimization analysis of the motor, the suggested method was to vary the airgap between the stator and rotor. The new value for the airgap was chosen from the optimetrics analysis in Ansys Maxwell which suggests the minimum value of the airgap that is possible without changing any other existing parameter. The minimum airgap which was suggested was 0.325 mm.

The comparison of the acceleration response for the same RPM and different airgap is shown in the figure below:

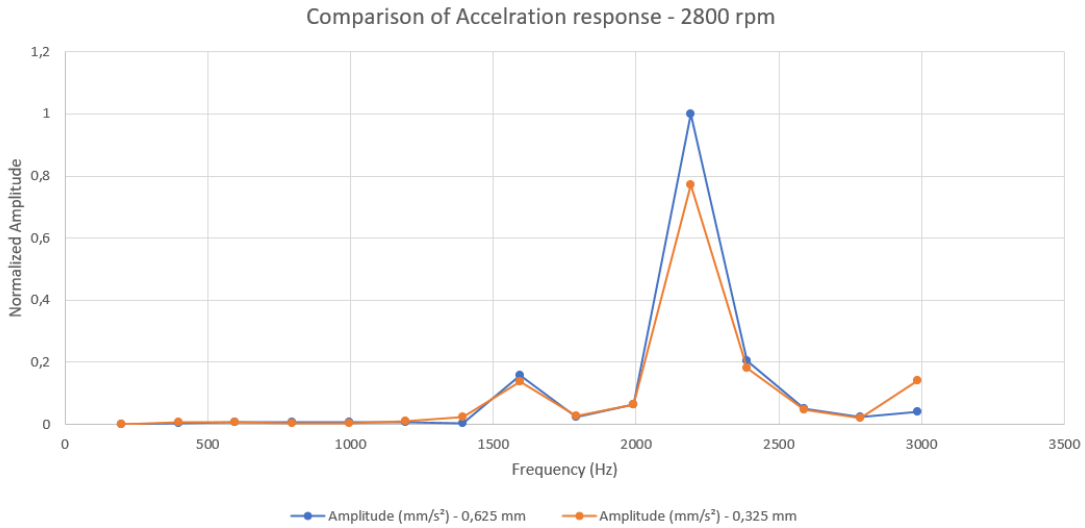

Figure 4.13: Comparison of acceleration response for 2800 RPM

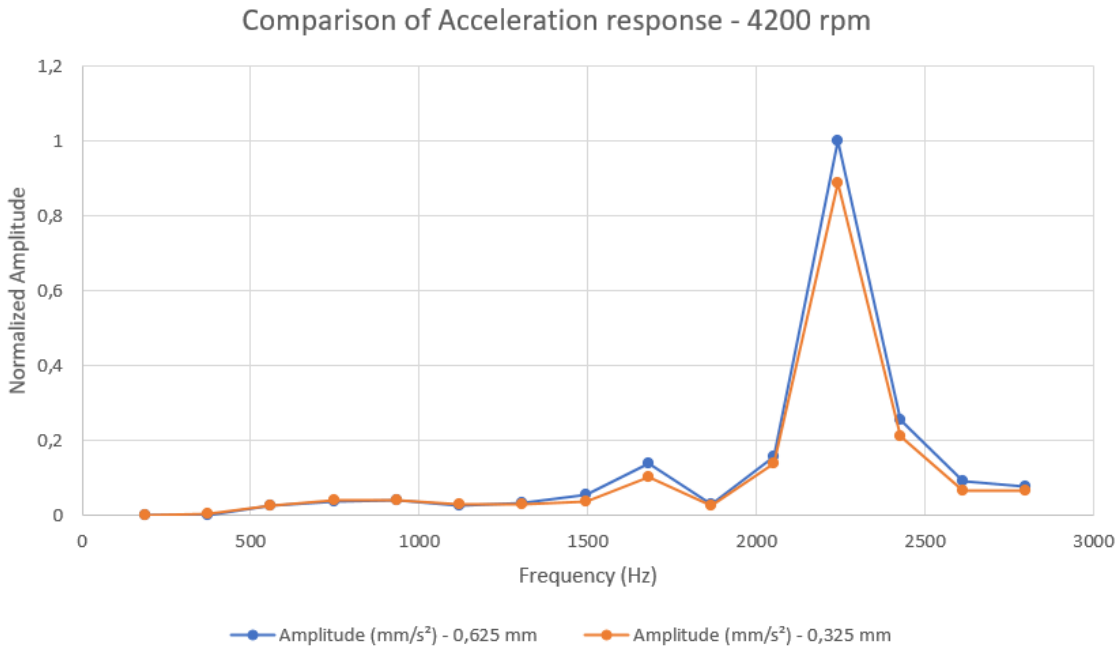

Figure 4.14: Comparison of acceleration response for 4200 RPM

It can be observed from Figures 4.13 and 4.14 that the acceleration response for both the RPMs follows the same trend. The acceleration is maximum at the same frequency for both the airgaps. The maximum acceleration is lesser for the 0.325 mm airgap. This can be attributed to the fact that lesser airgap means lesser magnetic flux lines pass through the airgap which slightly reduces the electromagnetic forces acting on the stator teeth.

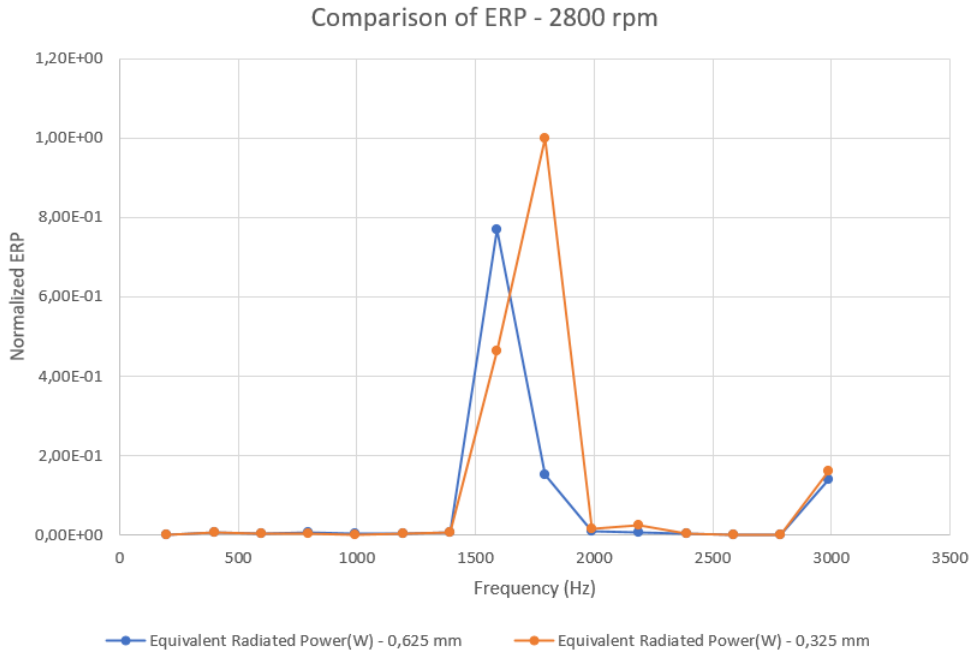

Figure 4.15: Comparison of Equivalent Radiated Power for 2800 RPM

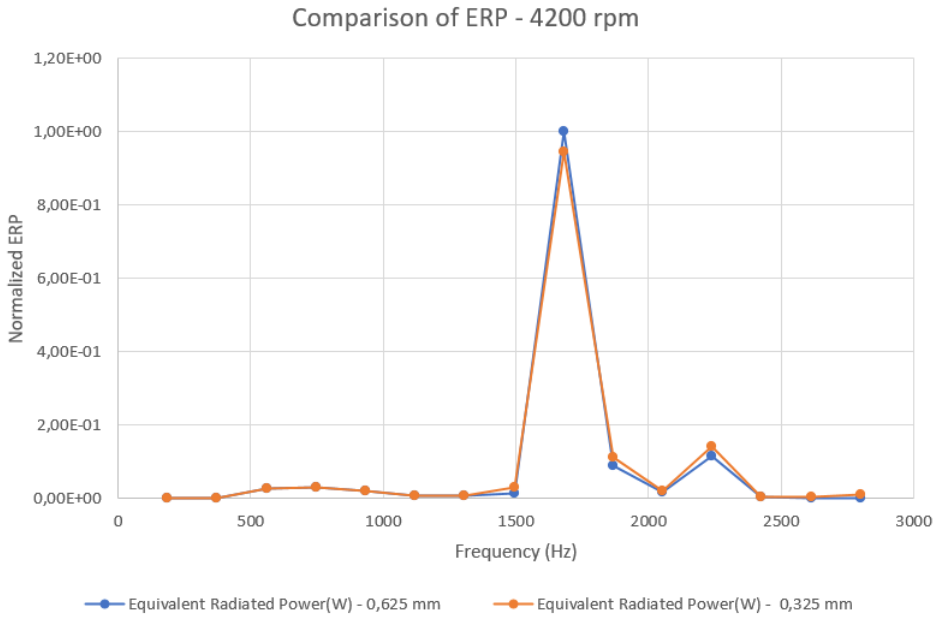

Figure 4.16: Comparison of Equivalent Radiated Power for 4200 RPM

From Figures 4.15 and 4.16 it is seen that the Equivalent Radiated Power for 2800 RPM for 0.625 mm and 0.325 mm airgap do not attain their peaks at the same frequency and the peak for 0.325 mm airgap is also higher than 0.625 mm airgap. This is an anomaly and further analysis is needed to understand why this phenomenon occurs.

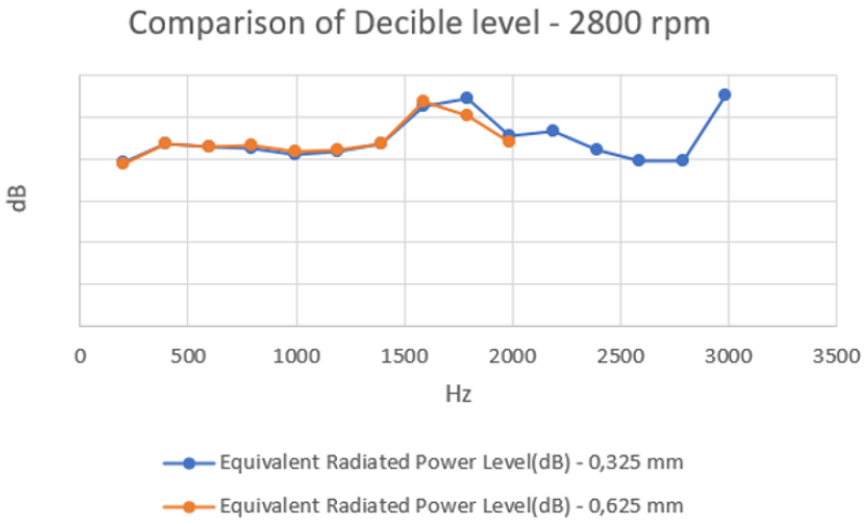

Figure 4.17: Comparison of decibel levels for 2800 RPM

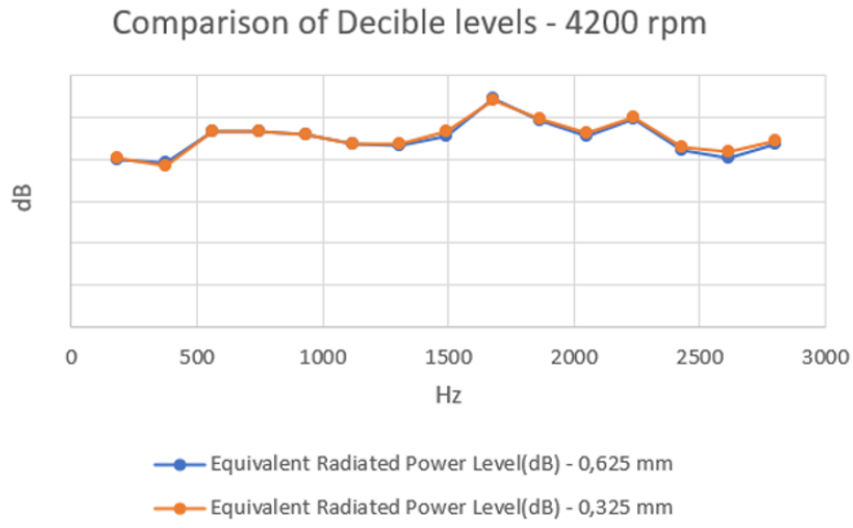

Figure 4.18: Comparison of decibel levels for 4200 RPM

From Figures 4.17 and 4.18, we can observe that the decibel levels for both the airgaps is almost identical for 4200 RPM where as there is a slight variation for 2800 RPM. This is due to the different peaks in the Equivalent Radiated Power graph shown in Figure 4.15. The reason for this difference in peaks should be investigated further.

5
Conclusion

The source of noise and vibration in an electric motor due to electromagnetic sources are the radial force, tangential force and the torque ripple. We have seen in table 3.6 that the radial force is much higher than the tangential force. The primary conclusions from this thesis work are :

- The acceleration response is directly affected by the electromagnetic forces acting on the stator teeth
- As the RPM increases there is a back emf induced in the coils which affect the electromagnetic forces acting on the stator teeth. Hence, as the RPM increases the amplitude of the acceleration response decreases.
- However, the RPM value has only been increased till the ideal operating range. The impact of the induced back emf after this range has to be studied.
- Equivalent Radiated Power gives a good estimate of the frequency at which the maximum sound will be emitted
- Equivalent Radiated Power is only accurate for lower frequencies, till the first resonance frequency to be specific, as after the first resonance frequency acoustic short circuit occurs
- Decreasing the airgap size decreases the amplitude of the acceleration response. However, this does not significantly affect the noise emitted from the motor.

6

Recommendations for future work

The recommendation for future work are :

- The thermal module in MotoCAD can be considered to see whether the permanent magnets are getting heated during operation and the effect of heating of the magnets and the windings on the magnetic flux density
- More than one parameter can be considered for the optimization of the electric motor. For example, the stator teeth thickness.
- Analyse the Equivalent Radiated Power for the entire housing and check the areas which has a higher power and optimize the geometry to reduce the noise emitted
- Export the results from waterfall diagram to Ansys Sound to hear the sound of the motor while in operation

Bibliography

[1] PMSM,
https://se.farnell.com/motor-control-permanent-magnet-sync-motor-pmsm-technolog

[2] MotorCAD,
https://en.wikipedia.org/wiki/Motor-CAD

[3] MotorCAD Brochure,
https://www.motor-design.com/wp-content/uploads/
About-Ansys-Motor-CAD-Brochure.pdf

[4] Senousy, M., Larsen, P., and Ding, P., "Electromagnetics, Structural Harmonics and Acoustics Coupled Simulation on the Stator of an Electric Motor," SAE Int. J. Passeng. Cars - Mech. Syst. 7(2):2014, doi:10.4271/2014-01-0933.

[5] Dupont, J., Aydoun, R., and Bouvet, P., "Simulation of the Noise Radiated by an Automotive Electric Motor: Influence of the Motor Defects," SAE Int. J. Alt. Power. 3(2):2014, doi:10.4271/2014-01-2070.

[6] Devillers, E., Degrendele, K., Hecquet, M., Lecointe, J.-P. et al., “Open-Access Testbench Data for NVH Benchmarking of E-Machines under Electromagnetic Excitations,” SAE Technical Paper 2019-01-1459, 2019, doi:10.4271/2019-01-1459.

[7] Zhang, H., Jaura, A., Kumar, D., Sambharam, T. et al., “Multiphysics Simulation of Electric Motor NVH Performance with Eccentricity,” SAE Technical Paper 2021-01-1077, 2021, doi:10.4271/2021-01-1077.

[8] Parmar, A., Miskin, A., Maheswar Rao, U., and Reddy, H.K., “Simulation Diagnostics Approach for Identification, Ranking and Optimization of Electric Motor Design Parameters for Optimal NVH Performance,” SAE Technical Paper 2021-01-1079, 2021, doi:10.4271/2021-01-1079.

[9] Ha, T.-W., Huh, J.-W., Choi, S.-K., Min, D.-W. et al., "Robust Development of Electric Powertrain NVH for Compact Electric SUV," SAE Technical Paper 2020-01-1503, 2020, doi:10.4271/2020-01-1503.

[10] 1 K. Wiechmann* , 2 J. Hiller 1 P+Z Engineering GmbH, Ingolstadt, Germany, 2 P+Z Engineering GmbH, Köln, Germany

[11] Simulation of vibrations in electrical machines for hybrid-electric vehicles
https://hdl.handle.net/20.500.12380/199927

[12] Structure–Acoustic Interaction Between Vehicle Floor Panels and Carpets – Numerical Simulations and Measurements
http://lup.lub.lu.se/student-papers/record/9061508

[13] Pierre Millithaler. Dynamic behaviour of electric machine stators : modelling guidelines for efficient finite-element simulations and design specifications for noise reduction. Structural mechanics [physics.class-ph]. Université de Franche-Comté, 2015. English. ffNNT : 2015BESA2003ff. fftel01316540
https://tel.archives-ouvertes.fr/tel-01316540

[14] Vibroacoustics of Electrical Drive Systems
https://doi.org/10.3929/ethz-b-000344764

[15] https://en.wikipedia.org/wiki/Faraday%27s_law_of_induction

[16] https://en.wikipedia.org/wiki/Amp%C3%A8re%27s_circuital_law

[17] https://en.wikipedia.org/wiki/Maxwell_stress_tensor

[18] https://www.azosensors.com/article.aspx?ArticleID=1956

A

Appendix 1

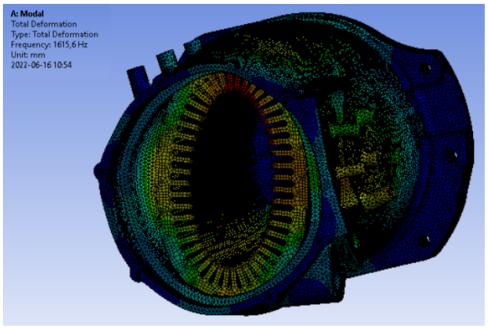
A: Modal
Total Deformation
Type: Total Deformation
Frequency: 1615,6 Hz
Unit: mm
2022-06-16 10:54

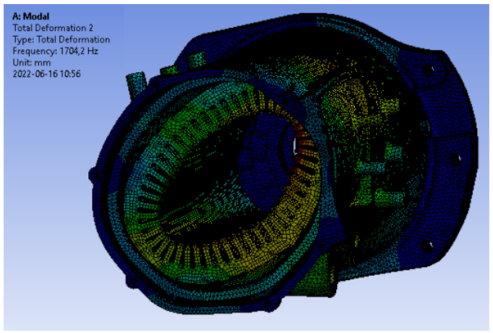
A: Modal
Total Deformation 2
Type: Total Deformation
Frequency: 1704,2 Hz
Unit: mm
2022-06-16 10:56

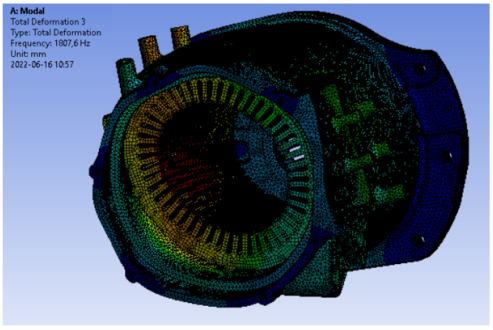
A: Modal
Total Deformation 3
Type: Total Deformation
Frequency: 1807,6 Hz
Unit: mm
2022-06-16 10:57

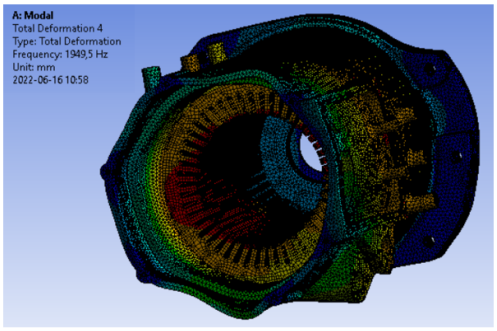
A: Modal
Total Deformation 4
Type: Total Deformation
Frequency: 1949,5 Hz
Unit: mm
2022-06-16 10:58

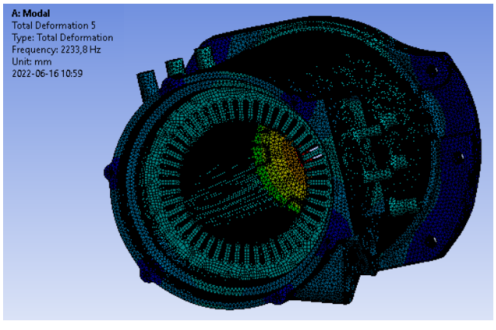
A: Modal
Total Deformation 5
Type: Total Deformation
Frequency: 2233,8 Hz
Unit: mm
2022-06-16 10:59

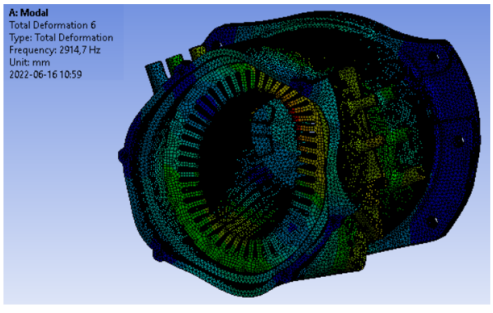
A: Modal
Total Deformation 6
Type: Total Deformation
Frequency: 2914,7 Hz
Unit: mm
2022-06-16 10:59

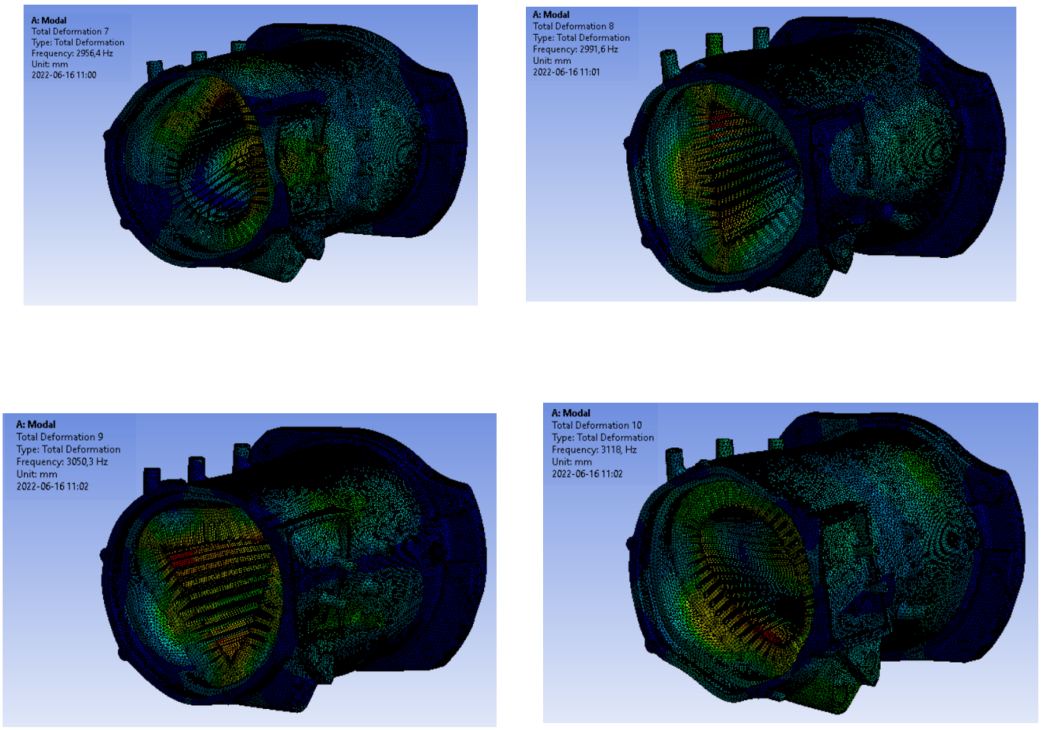

Figure A.1: First 10 resonant frequency modes

DEPARTMENT OF MECHANICS AND MARITIME SCIENCES
CHALMERS UNIVERSITY OF TECHNOLOGY
Gothenburg, Sweden
www.chalmers.se

CHALMERS
UNIVERSITY OF TECHNOLOGY